Reactions of $H_3O^+(H_2O)_{0,1}$ with Alkylbenzenes from 298 to 1200 K†

Anthony J. Midey,*,‡ Skip Williams, Susan T. Arnold, and A. A. Viggiano

Air Force Research Laboratory, Space Vehicles Directorate, 29 Randolph Road, Hanscom Air Force Base, Massachusetts 01731-3010

Received: November 12, 2001; In Final Form: October 1, 2002

Rate constants and branching fractions have been measured for the reactions of H_3O^+ and $H_3O^+(H_2O)$ with toluene (C_7H_8), ethylbenzene (C_8H_{10}), and *n*-propylbenzene (C_9H_{12}) as a function of temperature using a variable temperature-selected ion flow tube (VT-SIFT) and a high-temperature flowing afterglow (HTFA). The reactions have been studied up to 1200, 1000, and 900 K for toluene, ethylbenzene, and *n*-propylbenzene, respectively. The measurements are the first for $H_3O^+(H_2O)$ with these reactants. The H_3O^+ + alkylbenzene reaction rate constants are equal to the collision rate constants given by the Su−Chesnavich equation at all temperatures. Both nondissociative and dissociative proton-transfer products are observed. H_3O^+ reacts with toluene above 900 K to produce $C_7H_9^+$, $C_7H_7^+$, and $C_6H_5^+$ predominately, whereas only $C_7H_9^+$ is observed at lower temperatures. Proton transfer from H_3O^+ to ethylbenzene produces $C_8H_{11}^+$ exclusively at 300 K, and by 800 K, $C_6H_7^+$ is the major product with only minor amounts of $C_8H_{11}^+$ and $C_7H_7^+$ being formed. Both nondissociative and dissociative proton-transfer products are observed at all temperatures for H_3O^+ reacting with propylbenzene producing $C_9H_{13}^+$ as the major product at low temperatures and $C_6H_7^+$ and $C_3H_7^+$ as the major products at temperatures above 650 K, with minor amounts of $C_7H_7^+$ observed at all temperatures. For all three alkylbenzenes reacting with $H_3O^+(H_2O)$, nondissociative proton transfer dominates at low temperature; however, at 300 K, an association complex of all three alkylbenzenes with $H_3O^+(H_2O)$ is observed (14−18%). At higher temperatures, dissociative proton transfer is observed for $H_3O^+(H_2O)$ reacting with ethyl- and propylbenzene with similar product yields as observed in the H_3O^+ reactions. All of the $H_3O^+(H_2O)$ + alkylbenzene proton-transfer reactions are fast even though the proton affinity of $H_3O^+(H_2O)$ is 140 kJ mol^{-1} less than that of H_3O^+ making the $H_3O^+(H_2O)$ reactions endothermic. More specifically, the rate constant for the reaction of $H_3O^+(H_2O)$ with toluene is ca. half the collision rate constant at 300 K and equal to the collision rate constant at temperatures above 300 K even though the reaction is endothermic by 25 kJ mol^{-1}. Similarly, the reaction rate constants for $H_3O^+(H_2O)$ reacting with ethyl- and propylbenzene are equal to the collision rate constant at all temperatures despite being endothermic by 21 and 19 kJ mol^{-1}, respectively. Therefore, predictions based simply on reaction energetics would severely underestimate the reactivity of $H_3O^+(H_2O)$ with these alkylbenzenes. The possibilities of neutral water dimer production, ligand switching, uncertainties in the thermochemical data, and decomposition of the ionic products are considered to rationalize the observation of proton transfer where it is not thermodynamically feasible.

Introduction

Water is a key atmospheric constituent at low altitude and a major combustion product. The hydronium ion and numerous water clusters thereof, denoted as $H_3O^+(H_2O)_n$, are found in the atmosphere[1−3] and are quickly produced in humid air plasmas, often representing the bulk of the ionic species. In addition, H_3O^+ is known to exist in interstellar gases[3] and in the ionosphere.[2,4] Nevertheless, only the smallest of the protonated water clusters, i.e., $n = 0$ and 1, are stable in many high-temperature environments.[5]

The kinetics of a series of ion−molecule reactions with hydrocarbons have been studied using fast flow tubes at 298 K,[6−9] as have their temperature dependencies,[10−17] including the reactions of H_3O^+ with several alkanes up to 500 K using a variable temperature-selected ion flow tube (VT-SIFT).[11] However, no data exist on $H_3O^+(H_2O)$ reacting with these species. In fact, few studies of ion−molecule reactions involving protonated water clusters have been performed.[18−26] Recently, Adams and co-workers have studied the reactions of $H_3O^+(H_2O)_n$ for $n = 0$ and 1 with several thiol and sulfide compounds at 300 K in a selected ion flow tube (SIFT). Most notably, proton transfer has been observed to occur with $H_3O^+(H_2O)$ where it is not thermodynamically feasible, allowing for the investigation of the contributions of neutral water dimer production, entropy-driven reactions, and thermal dissociation.[20] Thermal dissociation processes have recently been studied in our laboratory at high temperatures using the high-temperature flowing afterglow (HTFA),[16] and entropy-driven reactions are an equally fertile topic.[20,27−29]

Recent changes to the HTFA apparatus make it possible to generate $H_3O^+(H_2O)$ for kinetics studies up to 1000 K. Both the VT-SIFT and the HTFA have been previously employed together for studying the rate constants and branching fractions of NO^+ and O_2^+ charge-transfer reactions with toluene (C_7H_8), ethylbenzene (C_8H_{10}), and *n*-propylbenzene (C_9H_{12}) to high temperatures.[16] The temperature dependencies of the branching fractions measured in this fashion have allowed us to construct breakdown curves and investigate the dissociation dynamics.[13,15,16] Consequently, the VT-SIFT and HTFA have been

† Originally submitted for the "Jack Beauchamp Festschrift", *J. Phys. Chem. A* **2002**, *106*, No. 42 (October 24).

* To whom correspondence should be addressed. E-mail: Anthony.Midey@hanscom.af.mil.

‡ Under contract to Visidyne, Inc., Burlington, MA.

10.1021/jp014141e CCC: $22.00
Published on Web 11/07/2002

utilized to measure rate constants and branching fractions for the reaction of $H_3O^+(H_2O)_n$ for $n = 0$ and 1 with toluene, ethylbenzene, and *n*-propylbenzene from 298 up to 1200, 1000, and 900 K, respectively. The dissociation dynamics illustrated by comparison of the temperature dependencies of the two reactant ions are discussed.

Experimental Section

The experiments have been conducted using the VT-SIFT[30] and HTFA[31] instruments at the Air Force Research Laboratory. The instrumental methods have been discussed at length elsewhere[30,31] and will only be briefly outlined. However, recent modifications to the HTFA source region will be described in detail.

Ions are generated in the VT-SIFT in a high-pressure source region. Electron impact ionization of a sample of room-temperature water vapor introduced into an effusive ion source generates ions. The desired reactant ion is selected with a quadrupole mass spectrometer and injected into a fast flow of helium buffer gas by way of a Venturi inlet. The neutral reactant gas is introduced downstream where it reacts over a known distance. The neutral reactant and product ions are sampled through a nose cone aperture and resolved with a second quadrupole mass analyzer and then detected with an electron multiplier. An excess of reagent gas is used so that the rate constants are determined through pseudo-first-order kinetics. The relative error in the rate constants is ±15%, and the absolute error is ±25%.[30]

The nascent product ion distributions are determined by extrapolating the branching fractions to zero neutral reactant flow to eliminate the effects, if any, arising from reactions of the product ions with the excess neutral reactant. The individual product branching fractions are determined in two steps. First, the branching fractions among the different C_n products are measured at low mass resolution to minimize mass discrimination, and then the branching fractions for each C_n peak are measured at high mass resolution to determine the branching between ions differing by a single mass unit. Corrections are made for the contribution of naturally occurring ^{13}C isotope peaks in the high-resolution experiments that overlap with higher mass ^{12}C products containing an additional H atom.[10] Figure 1a,b shows example mass spectra at low and high mass resolution for the reaction of $H_3O^+(H_2O)$ with ethylbenzene at 600 K in the HTFA.

Experiments are conducted similarly in the HTFA, except reactant ions are not mass-selected before the reaction zone. To expand the capabilities of the instrument, the entire cooled upstream region has been redesigned as shown in Figure 2. Previously, the ion source including all electrical and gas feedthroughs has been aligned coaxially with the flow tube. In the new design of Figure 2, the upstream region is a stainless steel tee that interfaces with the flow tube through a Teflon seal. A water-cooled copper heat exchanger chills the tee just upstream of this seal. The two ends of the tee make a continuation of the flow tube. The upstream end of the tee, which is coaxial with the flow tube, supports all of the flow tube gas feedthroughs including the pressure port, consisting of bent 0.25 in. o.d. industrial-grade quartz tubes that rest on the bottom of a 7 cm diameter industrial-grade quartz flow tube. The quartz tubes allow for operation up to 1400 K. For operation to 1800 K, the quartz tubes can be replaced with ceramic ones.

The sidearm of the tee shown in Figure 2 houses the new ion source region. A buffer gas enters the flow tube at the source flange, where a source gas can also be added through a second

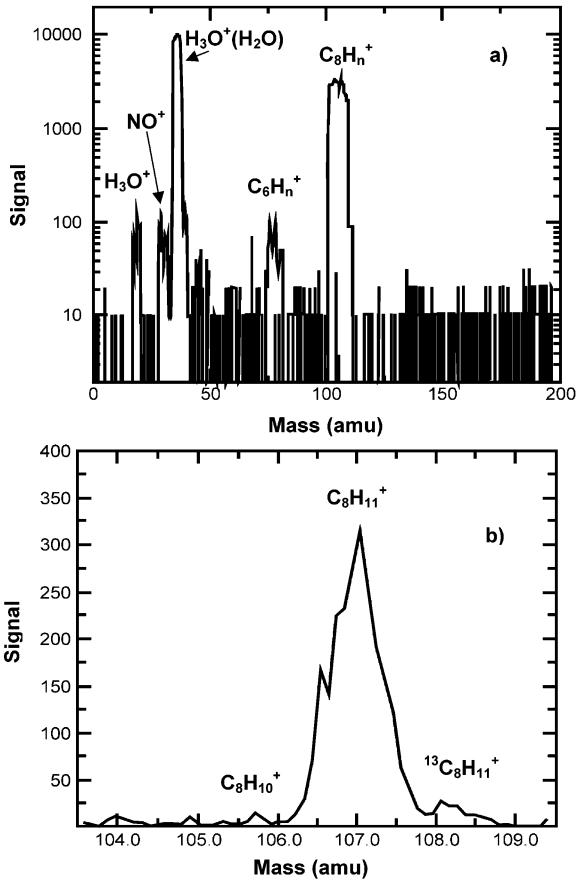

Figure 1. (a) Low-resolution mass spectrum showing the reaction of $H_3O^+(H_2O)$ with ethylbenzene (C_8H_{10}) in the high-temperature flowing afterglow (HTFA) using the new source design described in the Experimental Section and illustrated in Figure 2 and (b) high-resolution mass spectrum showing the individual C_8H_n peaks.

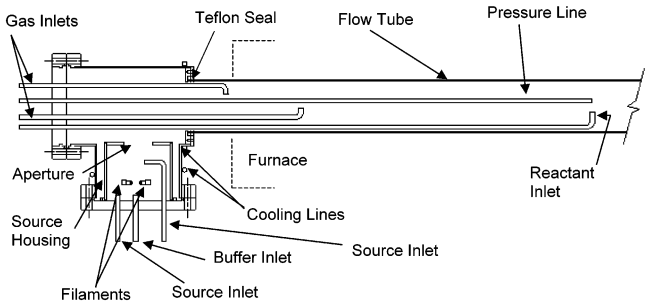

Figure 2. Newly designed upstream region of the high-temperature flowing afterglow (HTFA) including a redesigned source region. See text for details.

inlet. Downstream from the two inlets, a thoriated iridium filament creates ions. A third inlet allows gas to be added downstream of the filaments. In practice, one of two filaments is available. The filaments are connected to an external switch, reducing the number of times the flow tube must be opened to air for maintenance. Opening the system requires extensive outgassing of the firebrick in the furnace[31] for the system to be clean enough to measure branching fractions. The filament is biased with respect to the grounded tee, usually from 25 to 100 V. An emission regulator is used to control the level of ionization via the filament emission current.

When a helium buffer is used, He^+ and He* are produced through electron impact. An inlet downstream of the filament introduces a source gas that reacts with these energetic helium species to create the positive ion of interest. The entire source

resides inside a 3.5 in. diameter housing with a replaceable diaphragm. The aperture size has a variable diameter ranging from 0.125 to 1.25 in. to control the source pressure. The $H_3O^+(H_2O)$ experiments, for example, use a 0.25 in. diameter opening that results in a source pressure of approximately 20 Torr for typical buffer flows. For the H_3O^+ experiments, a 1 in. diameter aperture has been used.

The new upstream configuration provides several advantages. The ability to control the source pressure decreases the amount of source gas required to complete the reactant ion chemistry. This reduces the likelihood that additional reactions with the source gas will take place in the reaction zone, minimizing their contribution. Also, having the source in the sidearm results in a good shield for ultraviolet emissions from excited species generated in the source chemistry. This shielding has previously been done with baffles because ultraviolet light in the downstream region can create a diffuse source of ions throughout the reaction zone complicating the measurements.

The mass spectrum shown in Figure 1a was obtained using the new source configuration in the HTFA at a flow tube temperature of 600 K. Note that the ion intensity scale is logarithmic. The cluster ion accounts for over 95% of the total ion signal. To generate $H_3O^+(H_2O)$, helium carrier gas is bubbled through a water sample at room temperature and introduced into the source region downstream of the filaments. A needle valve controls the bubbler pressure to adjust the concentration of water vapor in the He/H_2O gas mixture. Average H_2O number densities in the source region of $(3-5) \times 10^{14}$ cm^{-3} occur under these conditions, which is much larger than the 2×10^{12} cm^{-3} H_2O number density present in the flow tube. The favorable operating conditions for generating $H_3O^+(H_2O)$ can be maintained from 500 to 800 K. Dissociation of the cluster increases above 800 K, giving larger amounts of H_3O^+ as the flow tube temperature increases. Consequently, no appreciable $H_3O^+(H_2O)$ signal can be generated over 1000 K. Below 500 K, higher order water clusters are also observed.

Clustering needs to be minimized to generate H_3O^+ cleanly in the HTFA. The first solvated species is quite stable and is readily produced even at the 0.5 Torr pressure in the flow tube. Thus, the amount of H_2O in the system needs to be minimized. However, energetic He species generated in the source region also need to be consumed. To address these concerns, the ions have been prepared as follows. A 1-in. diameter aperture has been used on the source, decreasing the source pressure to around 7−8 Torr at typical buffer flows. The buffer gas passes through a liquid nitrogen cooled sieve trap to remove water vapor to prevent additional cluster formation outside of the source region. A needle valve bleeds in room-temperature water vapor from a bulb, and it enters the flow tube at an inlet 10 cm inside the upstream heated end of the flow tube. Argon gas is added upstream of the filament, and hydrogen is added downstream of the filament. A simplified picture of the source chemistry is illustrated by eqs 1−3:[19]

$$He^* + Ar \rightarrow Ar^+ + He \quad (1)$$

$$Ar^+ + H_2 \rightarrow ArH^+ + H \quad (2)$$

$$ArH^+ + H_2O \rightarrow H_3O^+ + Ar \quad (3)$$

Argon reacts via Penning ionization with the energetic He species formed by electron impact on the buffer gas.[32] The Ar^+ ions then react with H_2 to give ArH^+ that is readily converted to H_3O^+. In addition, a number of other reactions of minor importance occur. ArH^+ also reacts with H_2 to produce H_3^+ that easily undergoes proton transfer with water.[19] Any H_2^+ ions generated react with Ar to give ArH^+ and with H_2 to form H_3^+, providing additional pathways for creating H_3O^+. In addition, Ar^+ charge transfers to H_2O, forming H_2O^+ that directly produces H_3O^+ via proton transfer and also reacts with H_2 to generate H_3^+.[19] Through the use of this complicated scheme, H_3O^+ ions comprise >80% of the ions in the flow tube with ca. 6% each of $H_3O^+(H_2O)$, O_2^+, and ArH^+, as well as ca. 2−3% total of N_2H^+ (from N_2^+ reacting with H_2 and H_2O) and trace amounts of H_3^+. Corrections for these species are made to the branching fractions as discussed later. Surprisingly, this reaction scheme is the cleanest way to make H_3O^+ in the HTFA. Other source conditions produce a larger fraction of impurity ions.

The alkylbenzene samples are all liquids with the following purities: toluene (Aldrich, 99+%), ethylbenzene (Aldrich, 99+%), and *n*-propylbenzene (Aldrich, 98+%). The samples are used as obtained from the manufacturer except for performing several freeze−pump−thaw cycles to remove trapped gases. The gases used are argon (AGA Gas, 99.999%), helium (AGA, 99.999%), and hydrogen (Air Products, 99.999%). The distilled water samples have been pumped on to remove dissolved gases.

Results

Table 1 shows the rate constants and branching fractions for the reactions of $H_3O^+(H_2O)_n$ for $n = 0$ and 1 with toluene, ethylbenzene, and *n*-propylbenzene from 298 to 500 K as measured in the VT-SIFT. The standard reaction enthalpies at 298 K in kJ mol^{-1} have been calculated[33,34] and are also listed in Table 1. The total average energy available for reaction $\langle E_{rxn} \rangle$ in kJ mol^{-1} at a given flow tube temperature shown in Table 1 has been calculated using eq 4:

$$\langle E_{rxn} \rangle = \langle KE \rangle + \langle E_{rot}^{aromatic} \rangle + \langle E_{vib}^{aromatic} \rangle + \langle E_{rot}^{ion} \rangle + \langle E_{vib}^{ion} \rangle \quad (4)$$

where the average kinetic energy, $\langle KE \rangle$, and the average rotational energy in both the aromatic and ionic reactants are each $^3/_2(k_bT)$. The average vibrational energies for the ionic and neutral reactants represent ensemble averages over Boltzmann distributions in the harmonic approximation. The alkylbenzene vibrational frequencies have been previously calculated using Gaussian 98 for all normal modes.[16] The vibrational frequencies of $H_3O^+(H_2O)$ have been taken from the ab initio calculations of Schaefer and co-workers for the global minimum energy structure having C_2 symmetry.[35] Using their frequencies in the alternate C_s symmetry gives a total vibrational energy that differs by <1%. The vibrational frequencies for H_3O^+ are taken from the NIST-JANNAF thermochemical tables.[36]

The standard reaction enthalpies at 298 K in kJ mol^{-1} have been calculated[33,34] and are also listed in Tables 1−4. Discussions of the experimental results, particularly those involving the $H_3O^+(H_2O)$ reactant, depend on the energetics of the processes involved. Therefore, it is important to have an understanding of the uncertainty of the calculated reaction enthalpies. Unfortunately, good error limits are not readily available for the thermodynamic quantities found in compilations and reviews. The most important thermodynamic parameter determining the error in the reaction enthalpy of the nondissociative proton-transfer channels is the difference between the proton affinity of H_2O and that of the alkylbenzene, a quantity reported to 0.1 kcal mol^{-1}. Therefore, we estimate the maximum error to be 4 kJ mol^{-1} (1 kcal mol^{-1}) for the proton affinities. Other important quantities are the bond strengths of H_2O

TABLE 1: Rate Constant and Branching Fractions for the Reactions of $H_3O^+(H_2O)_{0,1}$ with Alkylbenzenes in the Variable Temperature-Selected Ion Flow Tube from 298−500 K[a]

			rate constants and branching fraction		
Ion	reactant	$\Delta H^\circ_{rxn,298}$	298 K	400 K	500 K
		Toluene (C_7H_8)			
⟨av tot *E*⟩			20	30	39
H_3O^+	products		2.3 [2.2]	2.4 [2.1]	2.0 [2.1]
	$C_7H_9^+ + H_2O$	−93	1.00	1.00	1.00
⟨av tot *E*⟩			25	40	59
$H_3O^+(H_2O)$	products		0.9 [1.7]		1.4 [1.6]
	$C_7H_9^+ + (H_2O)_2$	25	0.82		1.00
	$H_3O^+(H_2O)C_7H_8$		0.18		
		Ethylbenzene (C_8H_{10})			
⟨av tot *E*⟩			22	33	46
H_3O^+	products		2.5 [2.4]	2.6 [2.3]	2.5 [2.3]
	$C_8H_{11}^+ + H_2O$	−97	1.00	0.98	0.96
	$C_7H_7^+ + CH_4 + H_2O$	−88		0.02	0.04
⟨av tot *E*⟩			27	43	66
$H_3O^+(H_2O)$	products		1.6 [1.8]		1.6 [1.8]
	$C_8H_{11}^+ + (H_2O)_2$	21	0.83		1.00
	$H_3O^+(H_2O)C_8H_{10}$		0.17		
		n-Propylbenzene (C_9H_{12})			
⟨av tot *E*⟩			24	39	53
H_3O^+	products		2.5 [2.6]	2.4 [2.5]	2.3 [2.5]
	$C_9H_{13}^+ + H_2O$	−99	0.94	0.91	0.75
	$C_7H_7^+ + C_2H_6 + H_2O$	−76	0.06	0.09	0.10
	$C_6H_7^+ + C_3H_6 + H_2O$	41			0.06
	$C_5H_5^+ + C_4H_8 + H_2O$	291			0.01
	s-$C_3H_7^+ + C_6H_6 + H_2O$	42			0.07
⟨av tot *E*⟩			29	49	73
$H_3O^+(H_2O)$	products		1.8 [1.9]		1.8 [1.9]
	$C_9H_{13}^+ + (H_2O)_2$	19	0.86		1.00
	$H_3O^+(H_2O)C_9H_{12}$		0.14		

[a] The collision rate constants, k_c, are given in brackets next to the experimental values, both in units of 10^{-9} cm^3 s^{-1}. The standard reaction enthalpies at 298 K and the average total energy available at each temperature are both given in units of kJ mol^{-1}. Maximum errors in reaction enthalpies are ±12 kJ mol^{-1} for the nondissociative channels and ±15 kJ mol^{-1} for the dissociation channels. (See text for details).

TABLE 2: Rate Constants and Branching Fractions for the Reactions of $H_3O^+(H_2O)_{0,1}$ with Toluene in the High-Temperature Flowing Afterglow from 500 to 1200 K[a]

		H_3O^+						
		rate constants and branching fraction						
toluene (C_7H_8)	$\Delta H^\circ_{rxn,298}$	500 K	700 K	850 K	900 K	1000 K	1100 K	1200 K
⟨av tot *E*⟩		39	83	117	128	154	180	236
[k_c]					[2.1]	[2.1]	[2.1]	[2.1]
products					2.0	2.0	1.8	2.3
$C_7H_9^+ + H_2O$	−93				0.98	0.87	0.81	0.29
$C_7H_8^+ + H + H_2O$	236					<0.01		
$C_7H_7^+ + H_2^+ H_2O$	−35					0.09	0.13	0.49
$C_6H_6^+ + CH_3 + H_2O$	239				<0.01	<0.01	<0.01	0.04
$C_6H_5^+ + CH_4 + H_2O$	170				<0.01	0.02	0.05	0.18

		$H_3O^+(H_2O)$				
		rate constants and branching fraction				
toluene (C_7H_8)	$\Delta H^\circ_{rxn,298}$	500 K	700 K	850 K	900 K	1000 K
⟨av tot *E*⟩		59	107	149	163	194
[k_c]			[1.6]	[1.6]		[1.6]
products			1.6	1.6		1.5
$C_7H_9^+ + (H_2O)_2$	25	1.00	1.00	0.98		1.00
$C_7H_8^+ + H + (H_2O)_2$	361			<0.02		

[a] The collision rate constants, k_c, are given in brackets above the experimental values, both of which have units of 10^{-9} cm^3 s^{-1}. The standard reaction enthalpies at 298 K and the average total available energy at each temperature are both given in units of kJ mol^{-1}. Maximum errors in reaction enthalpies are ±12 kJ mol^{-1} for the nondissociative channels and ±15 kJ mol^{-1} for the dissociation channels. (See text for details).

bound to H_3O^+ and H_2O. The latter is well-known,[37−39] and the former has been measured often[5] and calculated at a high level of theory.[35] The errors in these values can be estimated to be at most 10 kJ mol^{-1}. This leads to an overall maximum error of ±12 kJ mol^{-1} for the nondissociative proton-transfer reaction enthalpies. For the dissociative channels, the main ionic products are protonated benzene, $C_6H_7^+$, and protonated propane, $C_3H_7^+$. The proton affinity for benzene and propane are well-established, and the neutral organic products are alkenes with well-known enthalpies of formation. Therefore, we estimate the maximum errors of the reaction enthalpies of the dissociative reaction channels to be ±15 kJ mol^{-1}.

TABLE 3: Rate Constants and Branching Fractions for the Reactions of $H_3O^+(H_2O)_{0,1}$ with Ethylbenzene in the High-Temperature Flowing Afterglow from 500 to 1000 K[a]

		H_3O^+						
		rate constants and branching fraction						
ethylbenzene (C_8H_{10})	$\Delta H^\circ_{rxn,298}$	500 K	600 K	650 K	700 K	800 K	900 K	1000 K
⟨av tot E⟩		46	72	84	96	121	150	180
[k_c]		[2.3]	[2.3]	[2.3]	[2.3]	[2.3]	[2.3]	[2.3]
products		2.4	2.7	1.7	2.6	1.9	1.9	2.4
$C_8H_{11}^+ + H_2O$	−97	0.99	0.94	0.83	0.68	0.19	0.01	0.01
$C_7H_7^+ + CH_4 + H_2O$	−88					0.02	0.01	0.02
$C_6H_7^+ + C_2H_4 + H_2O$	51	0.01	0.06	0.17	0.32	0.79	0.98	0.97

		$H_3O^+(H_2O)$								
		rate constants and branching fraction								
ethylbenzene (C_8H_{10})	$\Delta H^\circ_{rxn,298}$	500 K	600 K	650 K	700 K	750 K	800 K	850 K	900 K	1000 K
⟨av tot E⟩		66	91	105	120	134	150	168	185	220
[k_c]			[1.8]	[1.8]	[1.8]	[1.8]	[1.8]	[1.8]	[1.8]	[1.8]
products			1.5	1.7	1.5	2.0	2.2	1.8	1.8	1.6
$C_8H_{11}^+ + (H_2O)_2$	21	>0.99	0.96	0.93	0.75	0.53	0.30	0.25	0.12	0.01
$C_8H_{10}^+ + H + (H_2O)_2$	355		<0.02	<0.02	<0.01	<0.02				
$C_7H_7^+ + CH_4 + (H_2O)_2$	37	<0.01		<0.01		<0.01				
$C_6H_7^+ + C_2H_4 + (H_2O)_2$	169		0.02	0.05	0.24	0.45	0.68	0.74	0.88	0.99
$C_6H_6+ + C_2H_5 + (H_2O)_2$	356					<0.01	<0.02	<0.01		

[a] The collision rate constants, k_c, are given in brackets above the experimental values, both of which have units of 10^{-9} cm^3 s^{-1}. The standard reaction enthalpies at 298 K and the average toluene rovibrational energy at each temperature are both given in units of kJ mol^{-1}. Maximum errors in reaction enthalpies are ±12 kJ mol^{-1} for the nondissociative channels and ±15 kJ mol^{-1} for the dissociation channels. (See text for details).

TABLE 4: Rate Constants and Branching Fractions for the Reactions of $H_3O^+(H_2O)_{0,1}$ with *n*-Propylbenzene in the High-Temperature Flowing Afterglow from 500 to 900 K[a]

		H_3O^+						
		rate constants and branching fraction						
n-propylbenzene (C_9H_{12})	$\Delta H^\circ_{rxn,298}$	500 K	600 K	650 K	700 K	750 K	800 K	900 K
⟨av tot E⟩		53	84	96	111	125	140	172
[k_c]			[2.5]		[2.4]	[2.4]	[2.3]	[2.3]
products			2.0		2.1	2.0	2.0	2.8
$C_9H_{13}^+ + H_2O$	−99	0.90	0.49			0.01	0.04	0.03
$C_9H_{12}^+ + H + H_2O$	226	<0.01	<0.01		<0.01			
$C_7H_7^+ + C_2H_6 + H_2O$	−76	0.03			0.01	0.01	0.10	0.06
$C_6H_7^+ + C_3H_6 + H_2O$	41	0.03	0.29		0.62	0.58	0.53	0.51
$C_3H_7^+ + C_6H_6 + H_2O$	123	0.03	0.20		0.36	0.40	0.33	0.40
s-$C_3H_7^+ + C_6H_6 + H_2O$	42							

		$H_3O^+(H_2O)$						
		rate constants and branching fraction						
n-propylbenzene (C_9H_{12})	$\Delta H^\circ_{rxn,298}$	500 K	600 K	650 K	700 K	750 K	800 K	900 K
⟨av tot E⟩		73	103	117	135	151	169	207
[k_c]			[1.9]		[1.9]	[1.9]	[1.9]	[1.8]
products			1.6		2.4	2.5	2.2	2.2
$C_9H_{13}^+ + (H_2O)_2$	19	>0.98	0.63	0.25	0.10	0.04	0.03	0.02
$C_9H_{12}^+ + H + (H_2O)_2$	351	<0.01	<0.01					
$C_7H_7^+ + C_2H_6 + (H_2O)_2$	49	<0.01				0.01		
$C_6H_7^+ + C_3H_6 + (H_2O)_2$	159	<0.01	0.25	0.51	0.60	0.54	0.60	0.52
$C_6H_6+ + C_3H_7 + (H_2O)_2$	361	<0.01			<0.01			
$C_3H_7^+ + C_6H_6 + (H_2O)_2$	248							
s-$C_3H_7^+ + C_6H_6 + (H_2O)_2$	160	<0.01	0.11	0.24	0.29	0.41	0.37	0.46

[a] The collision rate constants, k_c, are given in brackets above the experimental values, both of which have units of 10^{-9} cm^3 s^{-1}. The standard reaction enthalpies at 298 K and the average toluene rovibrational energy at each temperature are given in units of kJ mol^{-1}. Maximum errors in reaction enthalpies are ±12 kJ mol^{-1} for the nondissociative channels and ±15 kJ mol^{-1} for the dissociation channels. (See text for details).

The magnitude of the temperature dependence of the reaction enthalpies has been estimated as well. For $C_6H_7^+$ formation with ethylbenzene at 1000 K and for both $C_3H_7^+$ and $C_6H_7^+$ formation with propylbenzene at 900 K, $\Delta H(T)$ has been calculated using eq 5

$$\Delta H(T) = \Delta H(298\text{K}) + \int_{298}^{T} \Delta C_p(T)\, \mathrm{d}T \qquad (5)$$

where the change in the constant-pressure heat capacity, $\Delta C_p(T)$, in eq 5 is

$$\Delta C_p(T) = \sum_{i}^{\text{products}} \upsilon_i\, C_p^i(T) - \sum_{j}^{\text{reactants}} \upsilon_j\, C_p^j(T) \qquad (6)$$

The temperature-dependent change in the constant-pressure heat capacity is summed over the individual reactants and products that have reaction coefficients of ν_i. The values of $C_p(T)$ for a gas are well-represented by the JANNAF polynomials given

by eq 7 that allow for nonideal behavior, where the coefficients are available in the literature.[34,40,41]

$$C_p(T)/R = a_1 + a_2T + a_3T^2 + a_4T^3 + a_5T^4 \qquad (7)$$

Unfortunately, the coefficients for $H_3O^+(H_2O)$ and $(H_2O)_2$ are unavailable. Therefore, $C_p(T)$ has been approximated using $C_v(T)$ calculated using the partition functions for translational, vibrational, and rotational energy levels assuming an ideal gas under the rigid rotor and harmonic oscillator approximations in the high-temperature limit as shown in eqs 8−10 for nonlinear polyatomic molecules.[42]

$$C_p(T) = R + C_v(T) \qquad (8)$$

$$C_v(T) = \frac{3R}{2} + \frac{3R}{2} + \sum_v (\Theta_v/T)^2 \frac{e^{-\Theta_v/T}}{(e^{-\Theta_v/T} - 1)^2} \qquad (9)$$

where the vibrational temperature, Θ_v, for vibrational mode v with frequency ω in cm^{-1} is

$$\Theta_v = hc\omega/k_B \qquad (10)$$

The vibrational frequencies used have been taken from the literature.[16,34,35,38] Both the JANNAF polynomial and partition function-derived values of $C_p(T)$ have been calculated for H_3O^+ reactions to compare the two methods, while only statistical mechanics has been used for $H_3O^+(H_2O)$. The corrected enthalpy of reaction has been calculated for dissociative proton transfer with C_8H_{10} to give $C_6H_7^+$ at 1000 K and with C_9H_{12} to give either $C_3H_7^+$ or $C_6H_7^+$ at 900 K, which are the maximum temperatures studied for each alkylbenzene.

The enthalpy corrections for temperature will be most accurate using the JANNAF polynomials to calculate $C_p(T)$. Including the corrections determined using eq 7 shows that the reaction enthalpy at the highest temperatures increases for all three H_3O^+ reactions by ≤ 3 kJ mol^{-1}, well within the error of the standard reaction enthalpies. The partition function approach indicates that the corrected reaction enthalpy also increases (i.e., more endothermic) by 18−20 kJ mol^{-1} for the H_3O^+ reactions. The more approximate partition function approach gives a much larger correction and can be used as an upper limit to the correction term. A similar increase of 18−20 kJ mol^{-1} is calculated using the partition function approach for the $H_3O^+(H_2O)$ reactions. This calculated increase is close to the maximum errors of ± 15 kJ mol^{-1} estimated for the enthalpies of these reactions. Therefore, the reaction enthalpies at 298 K are a fair estimate of the reaction energetics at the temperatures studied and are used in the discussions of the dissociation product distributions at high temperatures.

The rate constants in Table 1 measured for H_3O^+ with the three alkylbenzenes agree well with the SIFT measurements of Spanel and Smith at 298 K.[8] In all cases, the reactions proceed via proton transfer at the Su−Chesnavich collision rate within experimental error.[43−45] H_3O^+ undergoes nondissociative proton transfer exclusively with toluene up to 500 K, in contrast to ethylbenzene, which shows small amounts of dissociative proton transfer at 400 and 500 K. Increasing amounts of dissociation products are also observed with *n*-propylbenzene as the temperature increases from 298 to 500 K. $H_3O^+(H_2O)$ undergoes mainly nondissociative proton transfer from 298 to 500 K. In addition, association (14−18%) is also observed at 298 K with all three alkylbenzenes. The reaction of $H_3O^+(H_2O)$ at 400 K has not been studied because the rate constant is equal to the collision rate constant at 298 and 500 K, and the product branching fractions show that nondissociative proton transfer products predominate at 298 K and are the only products observed at 500 K.

Tables 2−4 show the results for $H_3O^+(H_2O)_n$ with $n = 0$ and 1 reacting with toluene, ethylbenzene, and *n*-propylbenzene, respectively, as measured in the HTFA. Decomposition of the aromatic reagent in the flow tube before reaction limits the maximum temperature at which reactions can be studied in the HTFA to 1300 K for toluene, 1000 K for ethylbenzene, and 900 K for *n*-propylbenzene. This upper limit has been indicated in previous charge-transfer reaction studies with these alkylbenzenes in the HTFA.[16] The reaction of H_3O^+ with toluene has been studied only up to 1200 K in the HTFA because H_3O^+ cannot be generated above 1200 K without large amounts of impurity ions present. Both the rate constants and branching fractions for the various systems are given in Tables 2−4.

The final HTFA branching fractions given in Tables 2−4 have been corrected as follows. The $H_3O^+(H_2O)$ branching fractions at temperatures $\leq$800 K at which the ion signal is >95% pure $H_3O^+(H_2O)$ have been corrected for small amounts of O_2^+ and NO^+ (<3% individually), of which the branching fractions with the three alkylbenzenes at high temperatures are known.[16] $H_3O^+(H_2O)$ is also present in nonnegligible amounts in the H_3O^+ studies because water cannot be completely eliminated from the flow tube. Therefore, the H_3O^+ branching fractions at 800 K and below have been corrected using the $H_3O^+(H_2O)$ branching fractions measured here. As discussed in the Experimental Section, additional small corrections have been made to the H_3O^+ branching fractions for N_2H^+, ArH^+, O_2^+, and H_3^+ impurities resulting from the source chemistry described. For N_2H^+ and H_3^+, the SIFT branching fractions of McEwan et al. at 298 K have been used.[46] The kinetics of ArH^+ reacting with alkylbenzenes have not been studied previously. However, the proton affinity of Ar is close to that for N_2.[47] Therefore, it is assumed that ArH^+ has an identical branching fraction as N_2H^+ to correct the data. While it is preferable to use high-temperature kinetic data for the corrections, each of these impurity ions individually contributes a small percentage of the total ions in the flow tube. Consequently, the total correction to a single product ion's branching fraction will be a relatively small fraction, typically around 0.03−0.06. The O_2^+ chemistry is easily corrected for using the aforementioned HTFA data at high temperatures.[16]

Differences between the branching fractions for the two reactant ions at the highest temperatures can provide information on the dissociation mechanism. To eliminate any complications from a lack of ion selection upstream in the HTFA, the source conditions are varied so that predominantly the $H_3O^+(H_2O)_{n=0,1}$ ions are generated in the flow tube at a given temperature. The two ions can be made in differing amounts depending on whether water vapor is added at the inlet downstream from the filaments in the source region or at the inlet 10 cm inside the heated flow tube. For this experiment, a 1 in. diameter aperture has been used in the source and no other gases besides He and H_2O have been added to the flow tube. Product branching fractions at low mass resolution are subsequently measured with two different ratios of H_3O^+ to $H_3O^+(H_2O)$. This method results in a set of two equations with two unknowns that can be solved for each product ion's low-resolution branching fraction. For this experiment and all of the flow tube measurements, the sampling voltage on the nose cone has been minimized to prevent break up of any association products and cluster ions. Scanning the mass spectrometer at high resolution verifies that OH^+, H_2O^+, and other impurity ions total <1%. In addition,

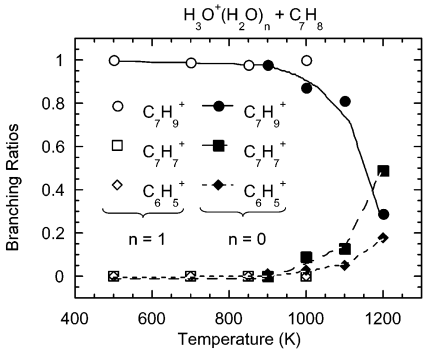

Figure 3. Branching fractions for the reaction of $H_3O^+(H_2O)_n$, $n = 0$ and 1, with toluene (C_7H_8) as a function of temperature as measured in the high-temperature flowing afterglow (HTFA). The solid symbols are the results for H_3O^+, and the open symbols are the results for $H_3O^+(H_2O)$. Lines are added to guide the eye.

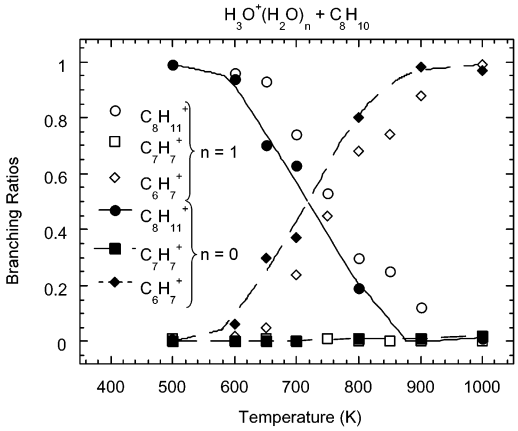

Figure 4. Branching fractions for the reaction of $H_3O^+(H_2O)_n$, $n = 0$ and 1, with ethylbenzene (C_8H_{10}) as a function of temperature as measured in the high-temperature flowing afterglow (HTFA). The solid symbols are the results for H_3O^+, and the open symbols are the results for $H_3O^+(H_2O)$. Lines are added to guide the eye.

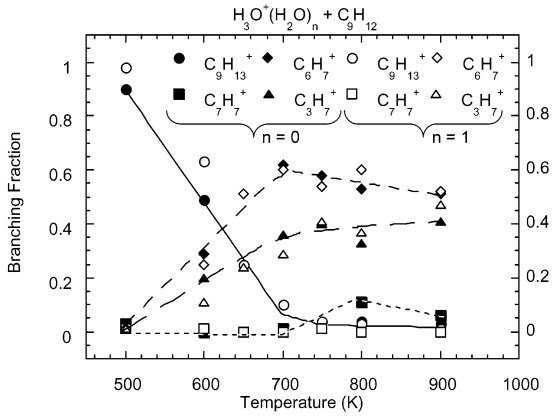

Figure 5. Branching fractions for the reaction of $H_3O^+(H_2O)_n$, $n = 0$ and 1, with *n*-propylbenzene (C_9H_{12}) as a function of temperature as measured in the high-temperature flowing afterglow (HTFA). The solid symbols are the results for H_3O^+, and the open symbols are the results for $H_3O^+(H_2O)$. Lines are added to guide the eye.

scanning the mass analyzer at high mass resolution under these experimental conditions shows that only one product ion arises for each C_n peak at high mass resolution for this experiment, simplifying the measurements. This procedure has been used to measure the branching fractions at 1000 K with toluene, 900−1000 K with ethylbenzene, and 750−900 K with *n*-propylbenzene. This method leads to smaller relative errors in the branching fractions than the normal method for measuring the separate branching fractions for each reactant ion.

Comparing the data from the VT-SIFT and HTFA reveals generally good agreement between the two methods, consistent with previous studies with a few exceptions.[13,15,16] Above 500 K, all of the reactions proceed at the Su−Chesnavich collision rate[43−45] within the error of the experiments. The scatter in the rate constants is larger for ethylbenzene and *n*-propylbenzene because of their low vapor pressures, making these reagents harder to deliver with our current flow meter arrangement. The biggest discrepancy is found in the H_3O^+ reaction with *n*-propylbenzene. Approximately 25% dissociation products occur in the VT-SIFT at 500 K, while only 10% is found in the HTFA. We have investigated the possible dependence of various experimental conditions that may differ between the two instruments such as nose cone sampling voltage, pressure, reaction time, buffer concentration, and mass discrimination and have not found an instrumental source of the discrepancy. Consequently, this difference remains unresolved, and an explanation for the difference is not obvious.

The branching fractions measured in the HTFA are plotted versus temperature for H_3O^+ and $H_3O^+(H_2O)$ in Figures 3−5 for toluene, ethylbenzene and *n*-propylbenzene, respectively. As the temperature increases, the fraction of dissociation products increases with both reactant ions. The main dissociative product ions with toluene are $C_7H_7^+$ and $C_6H_5^+$, while $C_6H_7^+$ is the major dissociation product with both ethyl- and *n*-propylbenzene. A substantial $C_3H_7^+$ fragment is also observed with *n*-propylbenzene. With toluene, nondissociative proton-transfer products are observed almost exclusively up to 1000 K with $H_3O^+(H_2O)$. This observation contrasts with the increasing amounts of dissociation products observed at 1000 K and higher with H_3O^+. Figures 4 and 5 show that the branching fractions for H_3O^+ and $H_3O^+(H_2O)$ display similar trends with increasing temperature for both ethylbenzene and *n*-propylbenzene, although the $H_3O^+(H_2O)$ curves are slightly shifted to higher temperatures. The nondissociative proton-transfer product is only a minor channel at 900 and 1000 K with ethyl and *n*-propylbenzene, respectively. Instead, the dominant product ions observed are $C_6H_7^+$ and $C_3H_7^+$, the latter only observed with *n*-propylbenzene.

Discussion

Nondissociative Proton Transfer. The main product channels for all of the reactions can be described as either nondissociative or dissociative proton transfer. At 298 K, the H_3O^+ reactions proceed at the Su−Chesnavich collision rate,[43−45] and nondissociative proton transfer is the major product channel. Adding a H_2O molecule to H_3O^+ causes the proton-transfer reactions to become endothermic because the ionic dimer bond ($H_3O^+-H_2O$) is much stronger than the neutral bond (H_2O-H_2O).[5] Despite this endothermicity, the $H_3O^+(H_2O)$ reactions are quite efficient at 298 K. Note that the calculated reaction endothermicities for the $H_3O^+(H_2O)$ nondissociative proton-transfer products are greater than the maximum estimated error in these values, suggesting that that these reactions are by no means exothermic. However, the average total energy available at 298 K (calculated from eq 4) is approximately equal to or greater than the endothermicity. Therefore, enough energy is available to drive the reactions if all forms of energy affect the reactivity equally. For instance, 25 kJ mol^{-1} average energy is available in the toluene reaction, compared to an endothermicity of 25 ± 12 kJ mol^{-1}. For this case, a rate constant

approximately $^1/_2$ the Su−Chesnavich collision rate constant is observed.[43−45] The total average energies in the ethyl and *n*-propylbenzene reactions exceed the reaction endothermicities by considerable margins, and the measured rate constants are close to collisional. If the energy required to overcome the endothermicity is provided by the internal and translational energy of the reactants, the products of these reactions would be internally cold.

It is possible that the protonated alkylbenzene species in the $H_3O^+(H_2O)$ reactions may be formed by an indirect mechanism. Ligand switching is exothermic for all of the reactions but is not observed, even though such reactions can often be facile. The nonobservation of a ligand-switching product may be a result of thermal dissociation of the H_2O ligand following the ligand switching as shown below.

$$H_3O^+(H_2O) + AB \rightarrow H^+(AB)H_2O + H_2O \quad (11a)$$

$$H^+(AB)H_2O + He \rightarrow H^+AB + H_2O + He \quad (11b)$$

Thermal dissociation reactions involving H_2O ligands have been observed relatively frequently in our laboratory if the ligand bond is weak. Unfortunately, the bond strength of H_2O bound to the protonated alkylbenzenes is unknown. The most similar species listed in the NIST Webbook is protonated benzene, $C_6H_7^+$, for which the H_2O cluster bond strength is <71 kJ mol^{-1}. Typically, thermal dissociation for species with bond strengths on the order of 65 kJ mol^{-1} or less at 298 K has been observed.[48−50] Therefore, thermal dissociation is possible and potentially likely at higher temperatures.

A similar process involves one-step dissociation of the association complex, that is,

$$H_3O^+(H_2O) + AB \rightarrow [H^+(H_2O)_2AB]^* \xrightarrow{He} H^+AB + 2H_2O \quad (12)$$

The overall process is endothermic, but it is exergonic at room temperature (i.e., $\Delta G° = \Delta H° - T\Delta S° < 0$). These reactions may be an example of what has been referred to as entropy-driven reactions in the literature.[20,27−29] However, this process may be better described as free-energy-driven reactions where the energy required for overcoming the endothermicity is supplied from the internal energy content of the complex, collisions with the surrounding He buffer gas, or both. Because an association complex is observed at 298 K, the lifetime of such a complex should be quite long ($>10^{-7}$ s), thus facilitating many collisions with the He buffer. Also, sufficient time should be available so that energy randomization will occur in the complex, indicating that the internal energy of the reactants should be very effective in promoting reaction.

Dissociative Proton Transfer. For all of the H_3O^+ reactions, at least one dissociative proton-transfer channel is exothermic, namely, the formation of the $C_7H_7^+$ ion. However, all of the dissociative channels require rearrangement and occur only at higher temperatures, indicating that barriers to the dissociation processes exist. In fact, large amounts of $C_7H_7^+$ are found only in the toluene reaction. For the $H_3O^+(H_2O)$ reactions, dissociative proton transfer is quite efficient, considering that the reactions are very endothermic even if the two water molecules are assumed to remain attached to form $(H_2O)_2$. Although, it is probable that interactions of $(H_2O)_2$ with the helium will dissociate it into two H_2O monomers in the flow tube. The possibility of the production of neutral dimers in similar reactions has been discussed previously.[20,29,51]

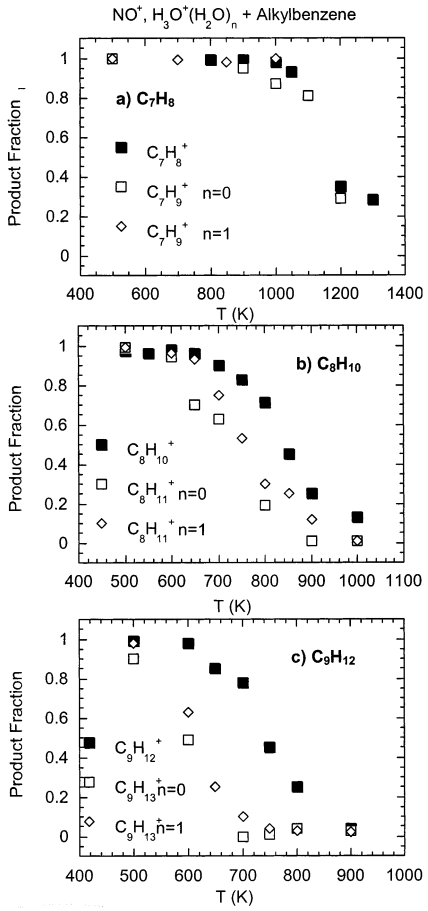

Figure 6. Branching fraction for the parent product ion of the reaction of NO^+ and $H_3O^+(H_2O)_n$ for $n = 0$ and 1 vs temperature for (a) C_7H_8, (b) C_8H_{10}, and (c) C_9H_{12}. Lines are added to guide the eye.

The temperature dependence of the nondissociative proton-transfer product for the reactions of toluene, ethylbenzene, and propylbenzene with H_3O^+ and $H_3O^+(H_2O)$ is shown in Figure 6. For comparison, the fraction of the nondissociative charge transfer product found previously in reactions of NO^+ [16] with these alkylbenzenes is also shown in Figure 6. In the previous charge-transfer work,[16] less than 2% of the total reactivity of toluene, ethylbenzene, and *n*-propylbenzene was attributed to thermal degradation of the neutral aromatic reactant prior to reaction at temperatures up to 1300, 1000, and 900 K, respectively. Hydrogen-depleted product ions appeared at high temperatures that were not observed in dissociative charge-transfer reactions at 298 K even with ions such as N_2^+ and Ne^+ that have large recombination energies that produce many fragments. These different products most likely result from reactions with the hydrogen-depleted decomposition products of the alkylbenzene reactant.[16] Pyrolysis data for these alkylbenzenes under our experimental conditions of ca. 1 Torr pressure of He and 1 ms residence time are limited, but the present results and the relative stability of these aromatic neutral species are consistent with the available data.[16] In Figure 6, the onset temperatures for dissociation of the charge-transfer products are higher than the onsets for the proton-transfer products, all of which are much lower than the pyrolysis temperatures for the neutrals reported previously.[16] Therefore, the decrease of the parent proton-transfer ion fraction, as well as the parent charge-transfer ion fraction, with temperature cannot be attributed to thermal degradation of the neutral alkylbenzene reactants.

Three mechanisms for the observed dissociative proton transfer can be envisioned, that is, direct dissociation in a bimolecular collision, nondissociative proton transfer followed by thermally activated unimolecular dissociation of the product ion involving the helium bath gas (hereafter referred to as thermal dissociation), and collisional activation of an association complex involving the reactants by collisions with the bath gas followed by dissociation (hereafter referred to as free-energy-driven dissociation). The three mechanisms are illustrated schematically in eqs 13a−c.

direct dissociation

$$H_3O^+(H_2O)_n + AB \rightarrow HA^+ + B + (H_2O)_n \quad (13a)$$

thermal dissociation

$$H_3O^+(H_2O)_n + AB \rightarrow HAB^+* + (H_2O)_n \quad (13b)$$

free-energy-driven dissociation

$$HAB^+ + He \rightarrow HAB^+* + He$$

$$HAB^+* \rightarrow HA^+ + B$$

$$H_3O^+(H_2O)_n + AB \rightarrow [H_3O^+(H_2O)_nAB]*$$

$$[H_3O^+(H_2O)_nAB]* + He \rightarrow HA^+ + B + nH_2O + He \quad (13c)$$

Comparing the data for H_3O^+ and $H_3O^+(H_2O)$ for the same neutral reactant as a function of temperature can help distinguish among these mechanisms. The energy difference for proton transfer for the two ions is 140 kJ mol^{-1}, with H_3O^+ being energetically favored. If dissociative proton transfer occurs in a single collision, that is, via a direct mechanism, the threshold for observing fragment ions should shift to higher temperature as the ion changes from H_3O^+ to $H_3O^+(H_2O)$ because less energy is available, assuming that all other aspects of the experiment are the same.

a. Toluene. Figures 3 and 6 show that no dissociation products are observed for the reaction of $H_3O^+(H_2O)$ with toluene up to 1000 K, while the H_3O^+ reaction with toluene shows an onset of dissociation around 900 K. Unfortunately, a comparison cannot be made at higher temperatures because of the instability of $H_3O^+(H_2O)$ above 1000 K in the HTFA. Subsequently, no information can be derived from this analysis on the nature of the dissociation in the $H_3O^+(H_2O) + C_7H_8$ reaction. The major fragment ion in the reactions of both NO^+ and H_3O^+ with toluene is $C_7H_7^+$. The $C_7H_7^+$ ion has two stable forms, the seven-membered ring tropylium ion (Tr^+) and the six-membered ring benzylium ion (Bz^+). The Tr^+ isomer is 46 kJ mol^{-1} more stable than the Bz^+ isomer.[33,34] The formation of the Tr^+ fragment ion via direct dissociation is exothermic for both NO^+ and H_3O^+ at 298 K. However, the $C_7H_7^+$ ion is not observed until much higher temperatures. The energetics for production of $C_7H_7^+$ via thermal dissociation are shown below where the He is shown above the arrow to illustrate the role of the bath gas:

$$C_7H_8^+ \xrightarrow{He} C_7H_7^+ + H \quad \Delta H = 166 \pm 8 \text{ kJ mol}^{-1} (Tr^+)$$
$$\Delta H = 212 \pm 8 \text{ kJ mol}^{-1} (Bz^+) \quad (14)$$

$$C_7H_9^+ \xrightarrow{He} C_7H_7^+ + H_2 \quad \Delta H = 63 \pm 8 \text{ kJ mol}^{-1} (Tr^+)$$
$$\Delta H = 109 \pm 8 \text{ kJ mol}^{-1} (Bz^+) \quad (15)$$

Activation energies can be determined from Arrhenius-type plots such as that shown in Figure 7a for toluene reacting with H_3O^+,

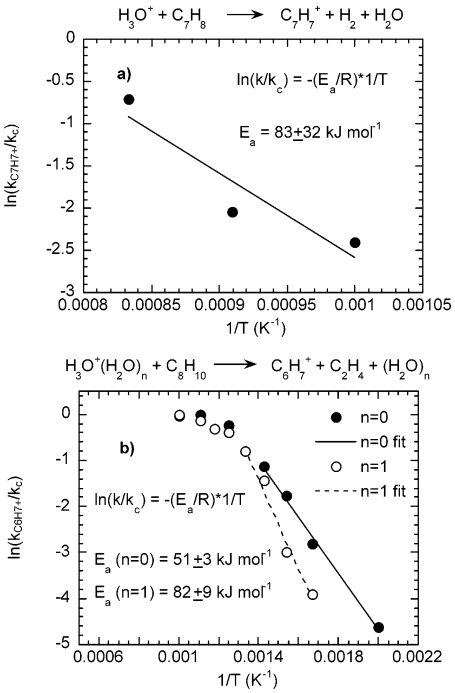

Figure 7. Arrehenius-type plot for (a) the reaction of H_3O^+ with toluene to produce $C_7H_7^+$ and (b) the reactions of H_3O^+ and $H_3O^+(H_2O)$ with ethylbenzene to produce $C_6H_7^+$.

yielding activation energies of 105 ± 10 kJ mol^{-1} and 83 ± 32 kJ mol^{-1} for the reactions of NO^+ and H_3O^+ with toluene, respectively. Note that the rate constant for generating a particular fragment channel is simply the product of the branching fraction for that channel with the experimental rate constant. The rate constants measured here are equal to the collision rate constant and are, thus, independent of temperature. Consequently, the temperature dependence of the rate constants for the $C_7H_7^+$ ion can be represented by just the branching fractions, because they will be multiplied by a constant factor in this case. Note that only the threshold region of the branching fraction plots is used to obtain the Arrhenius activation energies.

The formation of $C_7H_7^+$ in the NO^+ reaction with toluene has been attributed to thermal dissociation in our previous paper comparing flow tube results to ion beam results.[16] The ion beam work, performed under single-collision conditions, shows no fragmentation of the $C_7H_8^+$ charge-transfer product. In that work, the measured activation energy of 105 kJ mol^{-1} is lower than the endothermicity of reaction 14. However, the activation energy at low pressures, to which our experiments are limited, is smaller than the energy barrier because of the role of activation from internal degrees of freedom.[52−56] The measured activation energy for the formation of $C_7H_7^+$ from the reaction of H_3O^+ with toluene is larger than the endothermicity for the formation of the more stable Tr^+ isomer. This result suggests that either additional barriers exist in the unimolecular dissociation of $C_7H_9^+$ compared to $C_7H_8^+$ or that the activation energy corresponds to a barrier for the formation of $C_7H_7^+$ via a direct dissociation mechanism. The latter conclusion is consistent with the difference in the temperature dependence for the dissociation of $C_7H_9^+$ for the reactions of H_3O^+ and $H_3O^+(H_2O)$, which suggests that the H_3O^+ reaction proceeds via a direct mechanism.

b. Ethylbenzene and n-Propylbenzene. The ethylbenzene and *n*-propylbenzene reactions show similar behavior, with the *n*-propylbenzene dissociation shifted to lower temperatures. The

falloff in the protonated neutral species, that is, $C_8H_{11}^+$ and $C_9H_{13}^+$, occurs at temperatures of 40−50 K lower for H_3O^+ than for $H_3O^+(H_2O)$. The major dissociation product (>98%) in the ethylbenzene reaction is the $C_6H_7^+$ ion. Arrhenius-type plots up to temperatures of 750 K as shown in Figure 7b for the production of $C_6H_7^+$ from the reactions of H_3O^+ and $H_3O^+(H_2O)$ with ethylbenzene yield activation energies of 51 ± 3 and 81 ± 9 kJ mol^{-1}, respectively. At higher temperatures, the plots curve as the reaction rate constants approach the collision rate constant.

The activation energy of 51 ± 3 kJ mol^{-1} for H_3O^+ is equal to the endothermicity of 51 ± 10 kJ mol^{-1} within the uncertainties for the direct dissociative proton-transfer reaction given by

$$H_3O^+ + C_6H_5C_2H_5 \rightarrow C_6H_7^+ + C_2H_4 + H_2O, \quad \Delta H = 51 \pm 3 \text{ kJ mol}^{-1} \quad (16)$$

suggesting that direct dissociation is the dominant mechanism for this reaction channel. This equivalence of the activation energy and the reaction endothermicity has been seen previously for ion−molecule reactions.[57] On the other hand, the value of 81 ± 9 kJ mol^{-1} for the $H_3O^+(H_2O)$ activation energy is significantly lower than the endothermicity of 169 ± 13 kJ mol^{-1} for the direct dissociative proton-transfer reaction involving the $H_3O^+(H_2O)$ ion,

$$H_3O^+(H_2O) + C_6H_5C_2H_5 \rightarrow C_6H_7^+ + C_2H_4 + (H_2O)_2 \quad \Delta H = 169 \pm 13 \text{ kJ mol}^{-1} \quad (17)$$

as well as the value of 150 ± 8 kJ mol^{-1} for the thermal dissociation of the proton-transfer intermediate,

$$HC_6H_5C_2H_5^+ \xrightarrow{He} C_6H_7^+ + C_2H_4 \quad \Delta H = 150 \pm 8 \text{ kJ mol}^{-1} \quad (18)$$

Because the measured activation energy for $H_3O^+(H_2O)$ is significantly lower than the endothermicity of the direct process in reaction 17, it seems unlikely that the direct mechanism is contributing to a significant extent. Furthermore, a large amount of the $C_6H_7^+$ is produced at temperatures where the average total energy available is less than the endothermicity of the reaction. These data suggest that thermal activation of either the proton-transfer product, $C_8H_{11}^+$, or the association complex of the reactants, $H_3O^+(H_2O)C_8H_{10}$, is affecting the dissociation.

If thermal dissociation of the $C_8H_{11}^+$ proton-transfer product is responsible, the low value of the measured activation energy could arise from activation of internal degrees of freedom as discussed above for toluene,[52−56] resulting in products that are internally cool. On the other hand, the reaction may proceed via free-energy-driven dissociation involving the He buffer gas as shown below.

$$H_3O^+(H_2O) + C_8H_{10} \rightarrow [H^+(H_2O)_2C_8H_{10}]^* \xrightarrow{He} C_6H_7^+ + C_2H_4 + 2H_2O \quad (19)$$

To address this issue, the temperature at which a reaction becomes spontaneous, T_{spont}, has been calculated for the major dissociation products of the reaction of $H_3O^+(H_2O)$ with all three alkylbenzenes as shown in Table 5. The heats of formation[33,34,37] and entropies[58] used in the calculation are given in Table 6. It should be noted that the $S°$ values in Table 6 for $C_3H_7^+$ and $C_6H_7^+$ have been estimated using values for analogous neutral molecules. For the nondissociative proton-transfer ionic products, the entropies are estimated using similar neutral species. Most of the entropy values do not have errors given in the literature. However, for the few that are given, the error is <1 J mol^{-1} K^{-1}.[34] Considering that several of the entropies are estimated, we assume that the error in the standard entropies $S°$ given in Table 6 are ±1 J mol^{-1} K^{-1} and the errors in $\Delta S°_{rxn}$ in Table 5 are ±2 J mol^{-1} K^{-1}. Consequently, the errors in T_{spont} for the dissociative proton-transfer reactions in Table 6 are reported on the basis of the errors in $\Delta H°_{rxn}$ discussed earlier.

TABLE 5: Standard Enthalpies and Entropies of Reaction at 298 K[a]

reactants	products	$\Delta H°_{rxn}$ [b]	$\Delta S°_{rxn}$ [c]	T_{spont} (K)
	Toluene (C_7H_8)			
$H_3O^+(H_2O)$ →	$C_7H_9^+ + (H_2O)_2$	25	76	329 ± 167
	$C_7H_9^+ + 2H_2O$	40	154	260 ± 81
	Ethylbenzene (C_8H_{10})			
$H_3O^+(H_2O)$ →	$C_8H_{11}^+ + (H_2O)_2$	21	45	467 ± 287
	$C_8H_{11}^+ + 2H_2O$	36	123	293 ± 102
	$C_6H_7^+ + C_2H_4 + (H_2O)_2$	169	211	801 ± 69
	$C_6H_7^+ + C_2H_4 + 2H_2O$	184	288	639 ± 50
	n-Propylbenzene (C_9H_{12})			
$H_3O^+(H_2O)$ →	$C_9H_{13}^+ + (H_2O)_2$	19	53	386 ± 240
	$C_9H_{13}^+ + 2H_2O$	34	131	260 ± 96
	$C_6H_7^+ + C_3H_6 + (H_2O)_2$	159	220	723 ± 66
	$C_6H_7^+ + C_3H_6 + 2H_2O$	174	298	584 ± 48
	s-$C_3H_7^+ + C_6H_6 + (H_2O)_2$	160	207	773 ± 61
	s-$C_3H_7^+ + C_6H_6 + 2H_2O$	175	284	616 ± 43

[a] The maximum errors in reaction enthalpies are ±12 kJ mol^{-1} for the nondissociative channels and ±15 kJ mol^{-1} for the dissociation channels. The errors in the reaction entropies are ±2 J mol^{-1} K^{-1}. (See text for details). [b] kJ mol^{-1}. [c] J mol^{-1} K^{-1}.

TABLE 6: Standard Heats of Formation[a] and Entropies[b] at 298 K Used to Calculate the Spontaneous Temperature for Reaction Onset Shown in Table 5

species	$\Delta_f H°$ (kJ mol^{-1})	$S°$ (J mol^{-1} K^{-1})
$H_3O^+(H_2O)$	218 ± 9	253 ± 1
$(H_2O)_2$	−499[c] ± 2	300 ± 1
H_2O	−242 ± 1	189 ± 1
C_7H_8	50 ± 1	320 ± 1
$C_7H_9^+$	786 ± 8	350[d] ± 1
C_8H_{10}	30 ± 1	361 ± 1
$C_8H_{11}^+$	757 ± 8	360[d] ± 1
$C_6H_7^+$	863 ± 8	306[d] ± 1
C_2H_4	52 ± 1	219 ± 1
C_9H_{12}	8 ± 1	398 ± 1
$C_9H_{13}^+$	733 ± 8	405[d] ± 1
C_3H_6	20 ± 1	267 ± 1
$C_3H_7^+$	801 ± 4	289[c] ± 1
C_6H_6	83 ± 1	269 ± 1

[a] References 33 and 34. [b] Reference 58 and references therein. [c] Reference 37. [d] Estimated. See text for details.

Most ion−molecule reactions are bimolecular, yielding two or three products. Thus, the change in the number of molecules involved in the reaction, Δn, is either 0 or 1. For $\Delta n = 0$ reactions, typical entropy changes are ≤20 J mol^{-1} K^{-1}, while for $\Delta n = 1$ reactions, entropy increases are typically ~80 J mol^{-1} K^{-1}.[29] Reaction 19 is a candidate for a free-energy-driven reaction because it is a $\Delta n = 2$ reaction and is associated with a very large entropy increase of 288 J mol^{-1} K^{-1}, making the reaction exergonic at approximately 639 ± 50 K as shown in Table 5. For a free-energy-driven reaction, the energy to drive the reaction must come from the internal energy content of the complex, collisions with the bath gas, or both. The large endothermicity coupled with the large reaction efficiency

suggests that a significant fraction of the complexes undergo collisions with the bath gas. The observation of an association channel at 300 K indicates that stabilizing collisions of the helium bath gas with the complex are occurring. Because helium is an inefficient third body and there is a competing exothermic reaction, one may assume that many collisions are needed to observe a stabilized complex. Therefore, the complex lifetime at higher temperatures is expected to be long enough (>200 ns) to accommodate numerous collisions with the surrounding He bath gas during the interaction. Indeed, the data in Table 3 show that the onset of this channel occurs in the 600−650 K temperature range, consistent with the temperature calculated for ΔG to be negative, that is, 639 K.

A similar analysis can be applied to the dissociation of the *n*-propylbenzene proton-transfer intermediate, $C_9H_{13}^+$. In this reaction, a $C_3H_7^+$ fragment channel is observed in addition to the $C_6H_7^+$ fragment channel. The dissociation product channels for H_3O^+ reacting with *n*-propylbenzene are slightly endothermic,

$$H_3O^+ + C_6H_5C_2H_5 \rightarrow C_6H_7^+ + C_3H_6 + H_2O \quad \Delta H = 41 \pm 10 \text{ kJ mol}^{-1} \quad (20a)$$

$$\rightarrow s\text{-}C_3H_7^+ + C_6H_6 + H_2O \quad \Delta H = 42 \pm 7 \text{ kJ mol}^{-1} \quad (20b)$$

where the most stable secondary carbocation is created. These enthalpies are in reasonable agreement with the activation energies obtained from Arrhenius-type plots using the data at temperatures up to 700 K (using three points), which yield values of 45 ± 8 kJ mol^{-1} for $C_6H_7^+$ and 37 ± 7 kJ mol^{-1} for *s*-$C_3H_7^+$. A similar analysis of the fragments produced from the reaction of $H_3O^+(H_2O)$ with *n*-propylbenzene results in activation energies of 31 ± 10 kJ mol^{-1} for $C_6H_7^+$ and 33 ± 10 kJ mol^{-1} for *s*-$C_3H_7^+$, the same within the error. The product channels from $H_3O^+(H_2O)$ reacting with *n*-propylbenzene via direct dissociation of the proton-transfer complex are much more endothermic,

$$H_3O^+(H_2O) + C_6H_5C_3H_7 \rightarrow C_6H_7^+ + C_3H_6 + (H_2O)_2 \quad \Delta H = 159 \pm 13 \text{ kJ mol}^{-1} \quad (21a)$$

$$\rightarrow s\text{-}C_3H_7^+ + C_6H_6 + (H_2O)_2 \quad \Delta H = 160 \pm 11 \text{ kJ mol}^{-1} \quad (21b)$$

and they are even more endothermic than the thermal dissociation channels shown below,

$$HC_6H_5C_3H_7^+ \xrightarrow{He} C_6H_7^+ + C_3H_6 \quad \Delta H = 140 \pm 13 \text{ kJ mol}^{-1} \quad (22a)$$

$$\xrightarrow{He} s\text{-}C_3H_7^+ + C_6H_6 \quad \Delta H = 150 \pm 12 \text{ kJ mol}^{-1} \quad (22b)$$

Thus, the measured activation energies for the formation of $C_6H_7^+$ and $C_3H_7^+$ from the reaction of $H_3O^+(H_2O)$ with *n*-propylbenzene are much lower than the endothermicities listed for reactions 21a and 21b. This large difference makes the prospect of a direct process unlikely. Furthermore, the data in Table 4 show that by 750 K the $C_6H_7^+$ and $C_3H_7^+$ fragmentation channels combined are proceeding at 95% of the collision rate, implying that 95% of the reaction complexes have enough energy to react. At this temperature, the average energy available for reaction is approximately equal to the endothermicity, suggesting that actually less than 95% of the complexes have enough energy to react via a direct mechanism. However, if the differences in zero-point energy between the reactants and products are taken into account, ca. 60 kJ mol^{-1} of energy is also available for reaction.

A thermal dissociation mechanism for $H_3O^+(H_2O)$ with *n*-propylbenzene is more energetically favorable than direct dissociation for the $H_3O^+(H_2O)$ reactions and is possible, again through activation of internal degrees of freedom. The activation energies for the reaction of $H_3O^+(H_2O)$ with *n*-propylbenzene are so much lower than the endothermicities that free-energy-driven dissociation involving the He bath gas is also feasible. Indeed, the reactions listed in Table 5 for *n*-propylbenzene shown in eqs 23a and 23b

$$H_3O^+(H_2O) + C_9H_{12} \rightarrow [H^+(H_2O)_2C_9H_{12}]^* \xrightarrow{He} C_6H_7^+ + C_3H_6 + 2H_2O + He \quad (23a)$$

$$H_3O^+(H_2O) + C_9H_{12} \rightarrow [H^+(H_2O)_2C_9H_{12}]^* \xrightarrow{He} C_3H_7^+ + C_6H_6 + 2H_2O + He \quad (23b)$$

are exergonic at temperatures of 584 ± 48 and 616 ± 43 K, respectively. The observed onset for the two reaction channels as shown in Table 4 is between 500 and 600 K, in general agreement with these predictions. Again, the association complex of the reactants is observed at room temperature, indicating that numerous collisions with the He buffer are expected to occur for the complex even at high temperatures.

Conclusions

Rate constants and branching fractions have been measured for the reactions of H_3O^+ and $H_3O^+(H_2O)$ with toluene (C_7H_8), ethylbenzene (C_8H_{10}), and *n*-propylbenzene (C_9H_{12}) as a function of temperature up to 1200, 1000, and 900 K, respectively. The measurements are the first for $H_3O^+(H_2O)$ with these reactants. The H_3O^+ + alkylbenzene reaction rate constants are equal to the collision rate constants given by the Su−Chesnavich equation at all temperatures. The main product channels for all of the reactions can be described as either nondissociative proton transfer or dissociative proton transfer. H_3O^+ reacts with toluene to give only $C_7H_9^+$ at lower temperatures. Above 900 K, $C_7H_9^+$, $C_7H_7^+$, and $C_6H_5^+$ are seen predominately. Proton transfer from H_3O^+ to ethylbenzene produces $C_8H_{11}^+$ exclusively at 300 K, and by 800 K, $C_6H_7^+$ is the major product with only minor amounts of $C_8H_{11}^+$ and $C_7H_7^+$ being formed. Both nondissociative and dissociative proton-transfer products are also observed at all temperatures for H_3O^+ reacting with propylbenzene producing $C_9H_{13}^+$ as the major product at low temperatures and both $C_6H_7^+$ and $C_3H_7^+$ as the major products at temperatures above 650 K, with minor amounts of $C_7H_7^+$ observed at all temperatures.

For all three alkylbenzenes reacting with $H_3O^+(H_2O)$, nondissociative proton transfer dominates at low temperature. However, an association complex involving each alkylbenzene with $H_3O^+(H_2O)$ has been observed at 298 K comprising ca. 15% of the products. At higher temperatures, dissociative proton transfer is observed for $H_3O^+(H_2O)$ reacting with ethyl- and propylbenzene, in which the product yields are similar to those observed in the H_3O^+ reactions but they are shifted ~50 K higher. All of the $H_3O^+(H_2O)$ + alkylbenzene proton-transfer reactions are fast even though the proton affinity of $H_3O^+(H_2O)$ is 140 kJ mol^{-1} less than that of H_3O^+, such that the $H_3O^+(H_2O)$ reactions are endothermic. The existence of a stable association product with $H_3O^+(H_2O)$ at 298 K for all three

alkylbenzenes, coupled with the large rate constants proceeding at the thermal capture collision rate for both reactant ions,[43−45] indicates that the proton-transfer reactions involve a collision complex in the mechanism. Therefore, sufficient time should be available so that energy randomization will occur in the complex, indicating that the internal energy of the reactants should be very effective in promoting reaction. Also, the lifetime of the complex would be long enough to allow collisions with the He buffer gas to occur as well. This conclusion is consistent with the large proton-transfer rate constants for $H_3O^+(H_2O)$ listed in Tables 1−4, despite the endothermicity of these reactions. Temperature dependencies of the standard reaction enthalpies, as well as the errors in these values, have been eliminated as possible explanations.

Three mechanisms for generating the dissociative proton-transfer products observed with both reactant ions have been discussed: direct dissociation in a bimolecular collision, non-dissociative proton transfer followed by thermally activated unimolecular dissociation involving the helium bath gas, and formation of an association complex of the reactants followed by free-energy-driven production of endothermic product channels again likely involving the helium bath gas. Comparing the temperature dependencies of the H_3O^+ and $H_3O^+(H_2O)$ branching fractions, as well as the activation energies, shows that H_3O^+ reacts with all three alkylbenzenes via a direct dissociative proton-transfer mechanism. However, a small amount of $C_6H_5^+$ is observed at the highest temperatures studied with toluene that may result from thermal dissociation of the $C_7H_9^+$ proton-transfer intermediate. No dissociation has been observed for the reaction of $H_3O^+(H_2O)$ with toluene at temperatures up to 1000 K. Ethylbenzene reacts with $H_3O^+(H_2O)$ via either thermal or free-energy-driven dissociation in which the He buffer plays a role. Unfortunately, a definitive mechanism in the protonated water dimer ion reaction is not clear. In the reaction of H_3O^+-(H_2O) with *n*-propylbenzene, thermal dissociation is a possibility, as is free-energy-driven dissociation, both of which involve the helium bath gas present in the flow tube.

These measurements are the only high-temperature data available describing the proton-transfer kinetics of these alkylbenzenes. Extrapolations to high temperature using room temperature data or predictions based simply on reaction energetics would severely underestimate the contribution from dissociative reaction channels. However, the pressure dependencies of these reactions still need to be examined to better characterize the dissociation processes involved. A newly designed turbulent ion flow tube (TIFT) apparatus for kinetics measurements in the 100−760 Torr pressure range in our laboratory would prove beneficial for exploring pressure effects in these systems.[59,60] Time-resolved experiments would also provide important corroboration of one mechanism over the other, particularly those methods capable of probing the nascent product-state distributions.

Acknowledgment. We dedicate this paper to one of the pioneers in the field of ion chemistry, Jack Beauchamp. We thank Tom Miller for helpful discussions. We also thank John Williamson and Paul Mundis for technical support. A.J.M. is supported through Visidyne Contract Number F19628-99-C-0069. This work is supported by AFOSR under Task 2303EP4.

References and Notes

(1) Viggiano, A. A. *Mass Spectrom. Rev.* **1993**, *12*, 115−137.
(2) Viggiano, A. A.; Arnold, F. Ion Chemistry and Composition of the Atmosphere. In *Atmospheric Electrodynamics*; Volland, H., Ed.; CRC Press: Boca Raton, FL, 1995; Vol. 1, pp 1−25.
(3) Smith, D.; Spanel, P. *Mass Spectrom. Rev.* **1995**, *14*, 255−278.
(4) *Handbook of Geophysics and the Space Environment*; Jursa, A. S., Ed.; National Technical Information Service: Springfield, VA, 1985.
(5) Keesee, R. G.; Castleman, A. W., Jr. *J. Phys. Chem. Ref. Data* **1986**, *15*, 1011.
(6) Lindinger, W.; Hirber, J.; Paretzke, H. *Int. J. Mass Spectrom. Ion Processes* **1993**, *129*, 79−88.
(7) Spanel, P.; Pavlik, M.; Smith, D. *Int. J. Mass Spectrom. Ion Processes* **1995**, *145*, 177−186.
(8) Spanel, P.; Smith, D. *Int. J. Mass Spectrom.* **1998**, *181*, 1.
(9) Hansel, A.; Jordan, A.; Warneke, C.; Holzinger, R.; Lindinger, W. *Rapid Commun. Mass Spectrom.* **1998**, *12*, 871−875.
(10) Arnold, S. T.; Viggiano, A. A.; Morris, R. A. *J. Phys. Chem. A* **1997**, *101*, 9351−9358.
(11) Arnold, S. T.; Viggiano, A. A.; Morris, R. A. *J. Phys. Chem. A* **1998**, *102*, 8881.
(12) Arnold, S. T.; Morris, R. A.; Viggiano, A. A. *J. Phys. Chem. A* **1998**, *102*, 1345−1348.
(13) Arnold, S. T.; Williams, S.; Dotan, I.; Midey, A. J.; Morris, R. A.; Viggiano, A. A. *J. Phys. Chem. A* **1999**, *103*, 8421.
(14) Arnold, S. T.; Dotan, I.; Williams, S.; Viggiano, A. A.; Morris, R. A. *J. Phys. Chem. A* **2000**, *104*, 928−934.
(15) Midey, A. J.; Williams, S.; Arnold, S. T.; Dotan, I.; Morris, R. A.; Viggiano, A. A. *Int. J. Mass Spectrom.* **2000**, *195*, 327.
(16) Williams, S.; Midey, A. J.; Arnold, S. T.; Morris, R. A.; Viggiano, A. A.; Chiu, Y.-H.; Levandier, D. J.; Dressler, R. A.; Berman, M. R. *J. Phys. Chem. A* **2000**, *104*, 10336.
(17) Midey, A. J.; Williams, S.; Viggiano, A. A. *J. Phys. Chem. A* **2001**, *105*, 1574.
(18) Bohme, D. K.; Mackay, G. I.; Tanner, S. D. *J. Am. Chem. Soc.* **1979**, *101*, 3724.
(19) Ikezoe, Y.; Matsuoka, S.; Takebe, M.; Viggiano, A. A. *Gas-Phase Ion−Molecule Reaction Rate Constants Through 1986*; Maruzen Company, Ltd.: Tokyo, 1987.
(20) Williams, T. L.; Adams, N. G.; Babcock, L. M. *Int. J. Mass Spectrom. Ion Processes* **1998**, *172*, 149−159.
(21) Arnold, S. T.; Thomas, J. T.; Viggiano, A. A. *Int. J. Mass Spectrom.* **1998**, *179/180*, 243.
(22) Midey, A. J.; Arnold, S. T.; Viggiano, A. A. *J. Phys. Chem. A* **2000**, *104*, 2706.
(23) Morris, R. A.; Viggiano, A. A.; Arnold, S. T.; Paulson, J. F.; Liebman, J. F. *J. Phys. Chem.* **1995**, *99*, 5992.
(24) Viggiano, A. A.; Morris, R. A.; Van Doren, J. M. *J. Geophys. Res.* **1994**, *99*, 8221.
(25) Wincel, H.; Mereand, E.; Castleman, A. W. *J. Phys. Chem.* **1994**, *98*, 8606.
(26) Yang, X.; Zhang, X.; Castleman, A. W. *Int. J. Mass Spectrom. Ion Processes* **1991**, *109*, 339.
(27) Feng, W. Y.; Iraqi, M.; Lifshitz, C. *J. Phys. Chem.* **1993**, *97*, 3510−3514.
(28) Meot-Ner, M. *J. Phys. Chem.* **1991**, *95*, 6580−6585.
(29) Henchman, M. Entropy Driven Reactions. In *Structure/Reactivity and Thermochemistry of Ions*; Ausloos, P., Lias, S. G., Eds.; D. Reidel Publishing Company: Dordrecht, Holland, 1987; Vol. 193, pp 381−399.
(30) Viggiano, A. A.; Morris, R. A.; Dale, F.; Paulson, J. F.; Giles, K.; Smith, D.; Su, T. *J. Chem. Phys.* **1990**, *93*, 1149−1157.
(31) Hierl, P. M.; Friedman, J. F.; Miller, T. M.; Dotan, I.; Mendendez-Barreto, M.; Seeley, J.; Williamson, J. S.; Dale, F.; Mundis, P. L.; Morris, R. A.; Paulson, J. F.; Viggiano, A. A. *Rev. Sci. Instrum.* **1996**, *67*, 2142.
(32) Mitsuke, K.; Takami, T.; Ohno, K. *J. Chem. Phys.* **1989**, *91*, 1618.
(33) Lias, S. G.; Bartmess, J. E.; Liebman, J. F.; Holmes, J. L.; Levin, R. D.; Mallard, W. G. *J. Phys. Chem. Ref. Data* **1988**, *17* (Suppl. 1), 1−861.
(34) Lias, S. G.; Bartmess, J. E.; Liebman, J. F.; Holmes, J. L.; Levin, R. D.; Mallard, W. G. Ion Energetics Data. In *NIST Chemistry WebBook*; Mallard, W. G., Linstrom, P. J., Eds.; NIST Standard Reference Database Number 69; National Institute of Standards and Technology: Gaithersburg, MD, 1998; http://webbook.nist.gov.
(35) Xie, Y.; Remington, R. B.; Schaeffer, H. F. *J. Chem. Phys.* **1994**, *101*, 4878.
(36) Chase, M. W., Jr. *J. Phys. Chem. Ref. Data* **1998**, *9*, 1344.
(37) Curtiss, L. A.; Frurip, D. J.; Blander, M. *J. Chem. Phys.* **1979**, *71*, 2703.
(38) Frisch, M. J.; Pople, J. A.; Bene, J. E. D. *J. Phys. Chem.* **1985**, *89*, 3664.
(39) Lee, H. M.; Suh, S. B.; Lee, J. Y.; Tarakeshwar, P.; Kim, K. S. *J. Chem. Phys* **2000**, *112*, 9759.
(40) Kee, R. J.; Rupley, F. M.; Miller, J. A. *CHEMKIN II: A Fortran Chemical Kinetics Package for the Analysis of Gas-Phase Chemical Kinetics*; Sandia National Laboratories: Livermore, CA, April 1992.
(41) Burcat, A.; McBride, B. *1994 Ideal Gas Thermodynamic Data for Combustion and Air-Pollution Use*; TAE 697; Technion: Haifa, Israel, 1993.
(42) McQuarrie, D. A. *Statistical Mechanics*; Harper Collins: New York, 1976.

(43) Su, T.; Chesnavich, W. J. *J. Chem. Phys.* **1982**, *76*, 5183−5185.
(44) Su, T. *J. Chem. Phys.* **1985**, *82*, 2164−2166.
(45) Su, T.; Bowers, M. T. Classical Ion−Molecule Collision Theory. In *Gas-Phase Ion Chemistry*; Bowers, M. T., Ed.; Academic Press: New York, 1979; Vol. 1, pp 83−118.
(46) Milligan, D. B.; Wilson, P. F.; Freeman, C. G.; Meot-Ner, M.; McEwan, M. J. *J. Phys. Chem. A* **2002**, *106*, 9745−9755.
(47) Hunter, E. P.; Lias, S. G. Proton Affinity Evaluation. In *NIST Chemistry WebBook*; Mallard, W. G., Linstrom, P. J., Eds.; NIST Standard Reference Database Number 69; National Institute of Standards and Technology: Gaithersburg, MD, 1998; http://webbook.nist.gov.
(48) Hierl, P. M.; Ahrens, A. F.; Henchman, M.; Viggiano, A. A.; Paulson, J. F. *Int. J. Mass Spectrom. Ion Phys.* **1987**, *81*, 101.
(49) Arnold, S. T.; Morris, R. A.; Viggiano, A. A. *J. Chem. Phys* **1995**, *103*, 9242.
(50) Viggiano, A. A.; Arnold, S. T.; Morris, R. A. *Int. Rev. Phys. Chem.* **1998**, *17*, 147−184.
(51) Viggiano, A. A.; Morris, R. A.; Paschkewitz, J. S.; Paulson, J. F. *J. Am. Chem. Soc*. **1992**, *114*, 10477.
(52) Lovejoy, E. R.; Curtius, J. *J. Phys. Chem. A* **2001**, *105*, 10867−10873.
(53) Curtius, J.; Froyd, K. D.; Lovejoy, E. R. *J. Phys. Chem. A* **2001**, *105*, 10874−10883.
(54) Meot-Ner, M.; Field, F. H. *J. Am. Chem. Soc.* **1977**, *99*, 998.
(55) Meot-Ner, M.; Field, F. H. *J. Phys. Chem.* **1976**, *80*, 2665.
(56) Wayne, R. P. The Theory of the Kinetics of Elementary Gas-Phase Reactions. In *Comprehensive Chemical kinetics*; Wayne, R. P., Ed.; Elsevier Publishing Company: Amsterdam, 1969; Vol. 2, pp 256−275.
(57) Hierl, P. M.; Morris, R. A.; Viggiano, A. A. *J. Chem. Phys.* **1997**, *106*, 10145.
(58) Leung, K. M.; Lindstedt, R. P. *Combust. Flame* **1995**, *102*, 129.
(59) Arnold, S. T.; Seeley, J. V.; Williamson, J. S.; Mundis, P. L.; Viggiano, A. A. *J. Phys. Chem. A* **2000**, *104*, 5511.
(60) Arnold, S. T.; Viggiano, A. A. *J. Phys. Chem. A* **2001**, *105*, 3527.